Microsc. Microanal. 20, 164–174, 2014
doi:10.1017/S1431927613013937

Microscopy AND Microanalysis

Capturing Enveloped Viruses on Affinity Grids for Downstream Cryo-Electron Microscopy Applications

Gabriella Kiss,[1] Xuemin Chen,[1] Melinda A. Brindley,[2] Patricia Campbell,[3] Claudio L. Afonso,[4] Zunlong Ke,[5] Jens M. Holl,[1] Ricardo C. Guerrero-Ferreira,[1] Lauren A. Byrd-Leotis,[3] John Steel,[3] David A. Steinhauer,[3] Richard K. Plemper,[1,2] Deborah F. Kelly,[6] Paul W. Spearman,[1] and Elizabeth R. Wright[1,*]

[1]*Department of Pediatrics, School of Medicine, Division of Pediatric Infectious Diseases, Emory University, Children's Healthcare of Atlanta, Atlanta, GA 30322, USA*
[2]*Center for Inflammation, Immunity & Infection, Georgia State University, Atlanta, GA 30303, USA*
[3]*Department of Microbiology and Immunology, School of Medicine, Emory University, Atlanta, GA 30322, USA*
[4]*USDA, ARS, Southeast Poultry Research Laboratory, Athens, GA 30605, USA*
[5]*School of Biology, Georgia Institute of Technology, Atlanta, GA 30332, USA*
[6]*Virginia Tech Carilion Research Institute, Roanoke, VA 24016, USA*

Abstract: Electron microscopy (EM), cryo-electron microscopy (cryo-EM), and cryo-electron tomography (cryo-ET) are essential techniques used for characterizing basic virus morphology and determining the three-dimensional structure of viruses. Enveloped viruses, which contain an outer lipoprotein coat, constitute the largest group of pathogenic viruses to humans. The purification of enveloped viruses from cell culture presents certain challenges. Specifically, the inclusion of host-membrane-derived vesicles, the complete destruction of the viruses, and the disruption of the internal architecture of individual virus particles. Here, we present a strategy for capturing enveloped viruses on affinity grids (AG) for use in both conventional EM and cryo-EM/ET applications. We examined the utility of AG for the selective capture of human immunodeficiency virus virus-like particles, influenza A, and measles virus. We applied nickel-nitrilotriacetic acid lipid layers in combination with molecular adaptors to selectively adhere the viruses to the AG surface. This further development of the AG method may prove essential for the gentle and selective purification of enveloped viruses directly onto EM grids for ultrastructural analyses.

Key words: cryo-electron microscopy (cryo-EM), cryo-electron tomography (cryo-ET), affinity grid (AG), enveloped virus

Introduction

Enveloped viruses are a significant population of known viruses that are pathogens to both humans and animals. They are covered in a lipoprotein coat that is derived from the host cell's plasma membrane. Structural studies of enveloped viruses are essential because determining the overall architecture of the virus and common assembly pathways used by viruses may provide important information for antiviral research. Many enveloped viruses maintain a number of well-ordered macromolecular structures contained within the viral envelope, such as the capsid and the nucleocapsid. However, because the process of budding may be a reflection of host cell type, budding mechanism, or length of infection, most enveloped viruses exhibit a characteristic structural irregularity or pleomorphism. This structural variability can express itself as slight alterations to the size and internal architecture of the virus, such as with members of the *Retroviridae* family (Briggs et al., 2006*a*, 2006*b*; Wright et al., 2007, Butan et al., 2008; Carlson et al., 2008; Heymann et al., 2008; de Marco et al., 2010; Keller et al., 2011) to significant variations in the size and shape of the virus, as observed with members of the *Orthomyxoviridae* and *Paramyxoviridae* families (Harris et al., 2006; Yamaguchi et al., 2008; Loney et al., 2009; Calder et al., 2010; Lee, 2010; Liljeroos et al., 2011; Fontana et al., 2012; Liljeroos et al., 2013). Unfortunately, the structural heterogeneity of viruses may negatively impact the success of viral purification methods used for the production of highly concentrated viral samples, which are essential for cryo-electron microscopy (cryo-EM) and cryo-electron tomography (cryo-ET) studies.

Viruses for ultrastructural studies are produced through the transfection or infection of a permissive cell type. The growth of the virus is allowed to proceed for a required number of days. Following the incubation period, the cell culture supernatant or a combination of the supernatant and released cells are clarified by low-speed centrifugation. Subsequent steps of purification include the addition of chemicals to induce the precipitation of the virus; ultrafiltration by tangential flow techniques (Wickramasinghe et al., 2005); high-speed centrifugation through a dense-media cushion and/or a dense-media gradient; and a final dialysis or desalting step to remove excess contrast and ice quality distorting media (Mbiguino & Menezes, 1991; McGinnes et al., 2006; Gias et al., 2008). However, each of the purification methods may artificially select for viruses of a specific

Received August 4, 2013; accepted November 7, 2013
*Corresponding author. E-mail: erwrigh@emory.edu

size, density, or morphology; limit overall virus concentration (titer); alter the ultrastructure of the virus (Sugita et al., 2011); allow for the inclusion of cellular debris; or limit the probability of removing sucrose or other chemicals from the final preparation.

Recently, "monolayer purification" and "affinity grid" (AG) methods were introduced to the EM field in order to combine established His-tagged protein purification techniques directly with EM sample preparation and purification (Kelly et al., 2008*a*, 2008*b*). Briefly, AG are EM grids that have been coated with a lipid layer that contains a large percentage of nonfunctionalized lipids combined with a variable percentage of lipids that have the nickel-nitrilotriacetic acid (Ni-NTA) moiety. The Ni-NTA lipid binds directly to either the His-tagged protein of interest or to His-tagged Protein A that is bound to an antibody specific for the target protein. This technique has been successfully applied to the purification and structural analyses of ribosomes and RNA polymerase II from crude cell extracts (Kelly et al., 2010*b*), entire RNA processing pathways (Tanner et al., 2012), and the development of an *in situ* biological transmission electron microscopy (TEM) imaging platform (Gilmore et al., 2013). Here, we illustrate how AG technologies may be used to capture pleomorphic, enveloped viruses directly to EM grids that will be used for conventional TEM or cryo-EM/cryo-ET studies. The application of this technology for cryo-EM studies will provide novel prospects for imaging viruses that have otherwise been challenging under conventional methods.

Materials and Methods

Production and Purification of HIV Virus-Like Particles that Contain CD84

PCR fragments of codon-optimized HIV-1 Gag and HIV-1 JRFL Env were introduced sequentially into the plasmids pcDNA4/TO (Invitrogen, Carlsbad, CA, USA) and pcDNA5/TO(p) (the plasmid was modified by replacing the Hygromycin gene sequence of pcDNA5/TO with Puromycin gene to make a vector with a puromycin selection marker) to generate plasmid pcDNA4/TO Gag and pcDNA5/TO(p) Env. Expression of both Gag and Env in the plasmids pcDNA4/TO and pcDNA5/TO(p) Env is under a tetracycline-controlled cytomegalovirus promoter. The generation of stable cell lines expressing Gag and Env has been previously described (Hammonds et al., 2007; Hicar et al., 2010). For production of CD84-expressing HIV-1 virus-like particles (VLPs), the human CD84 gene was cloned into pcDNA5/TO vector to generate pcDNA5/TO CD84. PcDNA5/TO CD84 was transfected into a T-Rex293 Gag/Env stable cell line. The transfected cell lines were selected by using 200 μg/mL of hygromycin, 200 μg/mL of zeocin, and 1 μg/mL puromycin. The stable cell line after this selection produces HIV-1 Gag/Env VLPs with CD84 protein incorporated upon doxycycline induction.

HIV CD84 VLPs were harvested from individual clones after 2 days of 2 μg/mL doxycycline induction, clarified by low-speed centrifugation, and filtered through a 0.45 μm filter. At this point, the HIV VLP-containing solution was purified by one of two methods. In the first approach, the solution was further purified by ultracentrifugation through a 20% sucrose cushion (100,000 $\times$ g for 2 h, 4°C). In the second scheme, the solution was purified and concentrated 5$\times$ using Amicon Ultra-15 (100K) centrifugal filters (Millipore Corporation, Billerica, MA, USA) and then further concentrated by ultracentrifugation at 100,000 $\times$ g for 2 h at 4°C. Viral pellets from both methods were resuspended in 100 μL of PBS. The resuspended HIV CD84 VLPs were used for the imaging experiments. The concentrated solutions of HIV CD84 VLPs contain about 100 μg/mL of p24 (capsid protein) and 5μg/mL of gp120 (envelope glycoprotein).

Growth and Purification of Influenza Virus

For the propagation of influenza virus particles, 11-day-old pathogen free embryonated chicken eggs were infected with a 7:1 recombinant virus possessing seven segments of influenza A/Puerto Rico/34 (H1N1), and A/swine/Spain/53207/04 (H1N1) virus M segment (PR8, 7:1). The virus was generated by standard methods (Fodor et al., 1999) and exhibits a pleomorphic morphology. After incubation for 48 h at 37°C, the allantoic fluid was harvested and centrifuged at 1,700 $\times$ g for 10 min at 4°C to remove cell debris. The supernatant was then transferred to an ultracentrifuge tube and centrifuged at 12,000 $\times$ g for 30 min at 4°C. The clarified supernatant was layered on a 30% sucrose cushion and centrifuged at 77,000 $\times$ g for 1.5 h at 4°C. The pellet was resuspended in 100 μL of PBS overnight on ice. The sucrose was removed by dialysis for 6 h against PBS at 4°C. The final concentrated aliquots yielded titers of $\sim 10^8$ to $\sim 10^{10}$ PFU/mL.

Growth and Purification of Measles Virus

To generate a recombinant variant of measles virus (recMeV) variant harboring a triple Flag (Zhang et al., 2001) epitope-tagged hemagglutinin (H) protein, site-directed mutagenesis (QuikChange) was employed using a carboxy-terminally single Flag-tagged MeV H-Edmonston (Plemper et al., 2001) as template. The resulting H-Edm$_{3xFlag}$-encoding open reading frame (ORF) was sequence confirmed and transferred into a cDNA copy of the MeV-Edm genome, replacing the standard H ORF. Recombinant recMeV-H-Edm$_{3xFlag}$ virions were recovered as previously described (Plemper et al., 2001), and the presence of the epitope tag confirmed by immunoblot analysis of infected cell lysates using specific anti-Flag antibodies (M2; Sigma-Aldrich, St. Louis, MO, USA).

For virus production, ten 15 cm dishes of Vero-SLAM cells stably expressing human signaling lymphocyte activation molecule (Ono et al., 2001) were infected with recMeV-H-Edm$_{3xFlag}$ at a multiplicity of infection of 0.005. Released viral particles were collected when the cells showed more than 90% syncytia, $\sim$4 days postinfection. Supernatant was

clarified of cellular debris through a 0.45 μm filter and PEG precipitated by adding 10% PEG8000 and 2% NaCl to the final volume of the virus containing solution. The virus was then pelleted by centrifugation at 8,000 $\times$ g for 1.5 h at 4°C and the virus/PEG pellet gently resuspended in TNE buffer (10mM Tris, pH 7.5; 100mM NaCl; 1mM EDTA). Resuspended material was layered on a 20–60% sucrose cushion, centrifuged at 100,000 $\times$ g for 1.5 h, and viral particles collected from the interface of the 20–60% sucrose layers. To reduce the quantity of sucrose in the sample, the recovered virus-containing fraction was diluted in TNE buffer and centrifuged at 100,000 $\times$ g for 20 min. The pellet was then resuspended in TNE and centrifuged for a second time as above. The final pellet was resuspended in 200 μL of TNE and yielded titers of $\sim 10^7$ $TCID_{50}$ units/mL.

Preparation of Grids

Negatively Stained Grids

The 400 mesh carbon-formvar-coated copper grids (EM Sciences, Hatfield, PA, USA) were glow discharged for 30 s. Four μL of the virus sample was applied to the grid and allowed to adsorb for 1 min before staining for 30 s with either 2% methylamine tungstate (MAT) or 1% phosphotungstic acid (PTA).

Negatively Stained Affinity Grids

AG were prepared as described previously (Kelly et al., 2010*a*). Briefly, appropriate amounts of active [DGS-NTA(Ni); Avanti Polar Lipids, Alabaster, AL, USA] and filler lipids (DOPC; Avanti Polar Lipids) were mixed and added to the top of 15 μL distilled water drops. Lipid monolayers were formed after approximately 1 h incubation on ice. Nonglow discharged, 400 mesh, carbon-formvar-coated copper grids (EM Sciences) were placed carefully on the drops for 1 min to allow the affinity lipid monolayer to transfer and adhere. The grids with the affinity lipid monolayer attached were lifted and transferred to capillary tweezers. Aliquots (4 μL) of His-tagged protein A (Abcam, Cambridge, MA, USA) were applied to the monolayer and incubated for 1 min. The excess solution was removed using Whatman 1 filter paper. Immediately after blotting, 4 μL of virus-specific antibodies were applied to the grids for 1 min. The surplus solution was removed with filter paper and 4 μL of the virus suspension was deposited onto the grid and incubated for 2 min. The excess solution was removed with filter paper. The grids were washed four times to remove unbound particles before the negative stain was applied (2% MAT or 1% PTA).

Cryo-EM Grids

Quantifoil R1.2/1.3 carbon-copper grids (Quantifoil Micro Tools GmbH, Jena, Germany) were glow discharged for 30 s. Aliquots (4 μL each) of BSA-treated 10 nm gold particles (Sigma-Aldrich) were applied to the grids and allowed to air-dry. The virus sample (4 μL) was applied to the grid and allowed to disperse for 1 min. The grids were plunge-frozen using a FEI Mark III Vitrobot (FEI, Hillsboro, OR, USA).

Cryo-EM Affinity Grids

Quantifoil R1.2/1.3 carbon-copper grids were treated with ethyl acetate to remove plastic film residues. The monolayer was attached to the copper backside of the grid for greater stability. Solutions were applied to the monolayer as described for the negatively stained AG, excess solutions were pipetted away, no wash steps were performed. Virus sample (4 μL) was added to the grid and allowed to attach for 1 min. A second aliquot of the virus specimen was mixed in a 1:1 ratio with the BSA-treated 10 nm gold particles in a total volume of 2.5 μL and applied to the grid. The grids were plunge-frozen using a FEI Mark III Vitrobot.

EM

Negatively stained specimens were imaged on a JEOL JEM-1400 TEM (JEOL Ltd., Tokyo, Japan) equipped with a LaB_6 filament and operated at an accelerating voltage of 120 kV. Images with magnifications of 1,500, 4,000, and 12,000$\times$ were digitally captured on a Gatan US1000 (2k $\times$ 2k) CCD camera (Gatan, Pleasanton, CA, USA).

Vitrified specimens were either imaged on the JEOL JEM-1400 120 kV TEM, as described above, or the JEOL JEM-2200FS, 200 kV FEG-TEM with an in-column Omega energy filter operated at a slit width of 20 eV. Images on the JEOL JEM-2200FS were collected with a Gatan US4000 (4k $\times$ 4k) CCD camera. Images were automatically binned by two and acquired with a pixel size equal or less than 7.6 Å. For individual images, a total electron dose of ~ 5 $e^-/Å^2$ was used. For tilt series acquisition, a cumulative electron dose of ~ 120 $e^-/Å^2$ was distributed over tilt series ranging from $-62°$ to $+62°$. Images were acquired at -4.0 μm defocus (first CTF zero: 0.31 nm^{-1}). Tilt series images were automatically collected with angular increments of 2° using the predictive SerialEM package (Mastronarde, 2005).

Image Processing

Images from the negatively stained samples were used to quantify the number of viral particles present under each AG preparation method. Three-dimensional (3D) reconstructions (tomograms) were generated from the aligned image stacks using IMOD Version 4.3.1 (Kremer et al., 1996).

Virus and Particle Quantification

All particles in the field of view were counted in five 1,200$\times$ images acquired from each preparative condition for both the negatively stained grids and cryo-EM grids. For the unambiguous quantification of MeV on untreated cryo-grids and cryo-AG, all particles present were counted in five 3D reconstructions that were collected at a magnification of 30,000$\times$. Graphs represent the mean particle count from the five replicates; the standard deviations were calculated in Microsoft Office Excel. Particles were categorized as "viruses" if they displayed the characteristic viral mor-

phology that is known for each of the three viruses studied. In brief, a particle was classified as a virus if it maintained the general size and shape of each of the three viruses; had an intact viral envelope decorated with the virus-specific surface glycoproteins; and contained internal structural complexes consistent with each virus, such as the ribonucleoprotein (RNP) complex for MeV and influenza and the Gag lattice for the HIV VLPs. Particles not meeting the above criteria were categorized as "other particles."

Results and Discussion

HIV VLPs

HIV belongs to the *Retroviridae* family and is a modestly pleomorphic enveloped virus. We selected the HIV CD84 VLPs for the development of the affinity purification technique because the VLP morphology was relatively uniform; the Env glycoprotein or the CD84 moiety could be selectively targeted for binding; and high-affinity anti-Env (provided by Dr. Jason Hammonds) or CD84 (Santa Cruz Biotechnology, Dallas, TX, USA) antibodies were available. The VLPs were concentrated as described, then negatively stained and imaged (Fig. 1A; Supplementary Fig. 1A). The concentrated HIV VLP stock yielded images of intact, but densely packed VLPs on standard EM grids (Fig. 1A; Supplementary Fig. 1A). Solutions of the same HIV VLP stocks were then applied to the AG using the antibody/Protein A-His/Ni-NTA method. With all the viral systems studied, we examined if virus attachment could be selectively regulated by increasing the amount of the Ni-NTA lipid in the affinity monolayer from 2 to 20 to 50%. Intact HIV VLPs in negative stain TEM are identified by the presence of the Gag polyprotein layer. The HIV VLPs maintain a characteristic "doughnut- or red blood cell-like" morphology in which the spherical HIV VLPs "deflate" because of presence of the stain and slight dehydration from processing. Objects were categorized as "virus particles" that exhibited this morphological profile, while any particles not meeting this criteria were marked as "other particles." Due to the high density of particles in some conditions, we only quantified the number of whole visible particles at a magnification of 12,000× or greater. When using either the anti-Env antibody or the anti-CD84 antibody, the amount of HIV VLPs on the AG was dependent on the percentage of Ni-NTA lipid in the monolayer (anti-Env: Figs. 1B–1E; anti-CD84: Supplementary Figs. 1B–1E; Supplementary Tables 1, 2). Removal of either the Protein A-His or the antibody resulted in insignificant quantities of the HIV VLPs attached to the AG (Supplementary Figs. 2A, 2B; Supplementary Tables 1, 2). We applied a solution of 600 mM imidazole to the previously imaged AG and successfully eluted the HIV VLPs from the AG (Supplementary Fig. 2C; Supplementary Tables 1, 2) while retaining the intact lipid monolayer on the grid. Subsequently, fresh aliquots of HIV VLPs reattached to the AG monolayer at levels close to what was observed with first-round 20% AG (Supplementary Fig. 2D; Supplementary Tables 1, 2).

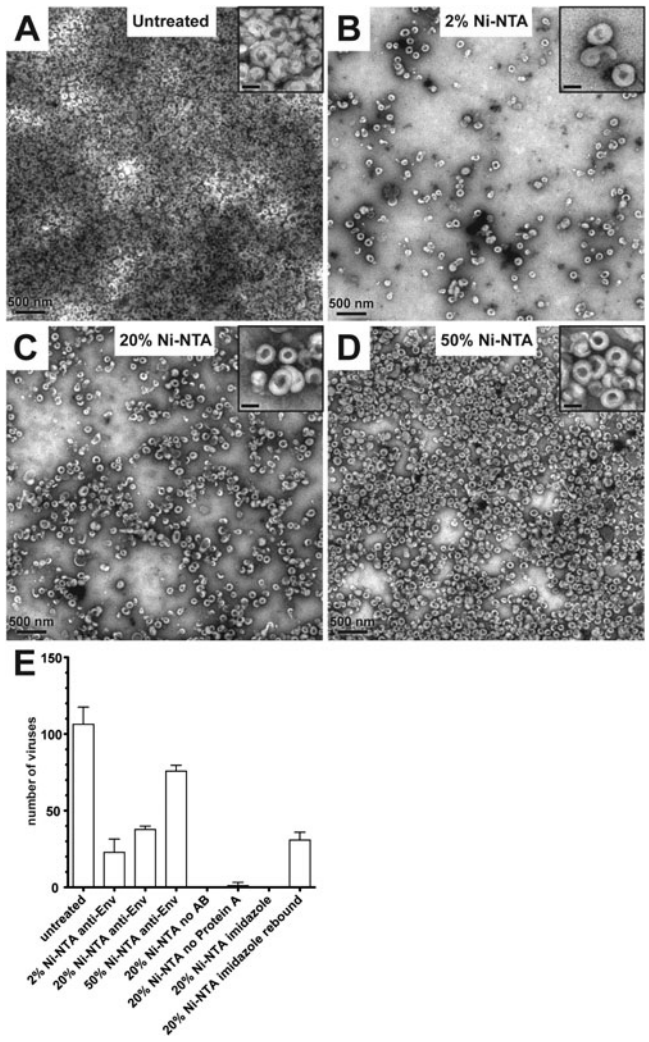

Figure 1. Transmission electron microscopy images of negatively stained human immunodeficiency virus (HIV) CD84 virus-like particles (VLPs). **A:** HIV CD84 VLPs from the resuspended pellet. **B:** HIV CD84 VLPs captured on a 2% nickel-nitrilotriacetic acid (Ni-NTA) affinity grid (AG) using an anti-Env polyclonal antibody (1:100). **C:** HIV CD84 VLPs captured on a 20% nickel-nitrilotriacetic acid (Ni-NTA) affinity grid using an anti-Env polyclonal antibody (1:100). **D:** HIV CD84 VLPs captured on a 50% Ni-NTA AG using an anti-Env polyclonal antibody (1:100). **E:** The number of HIV CD84 VLPs on untreated and AG electron microscopy (EM) grids. Untreated EM grids adsorbed more total VLPs than the three AGs. The AGs retrieved HIV CD84 VLPs proportionally to the percentage of the Ni-NTA present in the lipid monolayer. AG prepared without the anti-Env antibody or the protein A did not recruit VLPs to the grid surface. Treatment of the AG with 600 mM imidazole resulted in the elution of VLPs previously bound to the AG surface. HIV CD84 VLPs could be rebound to the AG surface after its treatment with imidazole. Images were acquired at 4,000 and 12,000× (insets) magnifications. Scale bars are 500 and 100 nm (insets).

Supplementary Material

To view Supplementary Figures 1–4 and Supplementary Tables 1–7 for this article, please visit http://dx.doi.org/10.1017/S1431927613013937.

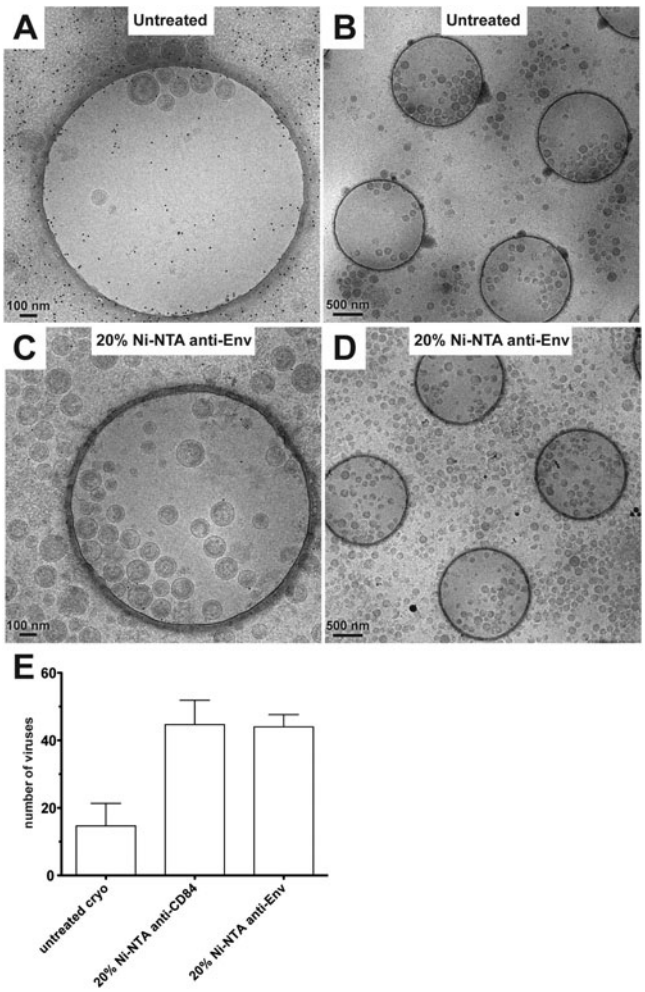

Figure 2. Cryo-electron microscopy (cryo-EM) images of human immunodeficiency virus (HIV) CD84 virus-like particles (VLPs). **A, B:** Cryo-EM images of HIV CD84 VLPs applied to a standard, untreated cryo-EM grid. **C, D:** Cryo-EM images of HIV CD84 VLP particles captured on a 20% nickel-nitrilotriacetic acid (Ni-NTA) cryo-affinity grid (cryo-AG) with an anti-Env polyclonal antibody (1:100). **E:** The amount of HIV CD84 VLPs on untreated and AG cryo-EM grids. Untreated EM grids adsorbed fewer HIV CD84 VLPs than the 20% Ni-NTA AG cryo-EM grid. Images were acquired at 30,000× (**A, C**) and 4,000× (**B, D**) magnifications. Scale bar: (**A, C**) 100 nm and (**B, D**) 500 nm.

We determined whether affinity purification techniques would be of benefit for cryo-EM studies of HIV VLPs. The use of the affinity monolayer on the cryo-EM grid resulted in more even distribution of the HIV VLPs across the entire grid as well as an overall increase in the number of HIV VLPs (Figs. 2D, 2E; Supplementary Table 3) as compared to a standard cryo-EM grid (Figs. 2A, 2B; Supplementary Table 3). This finding is of significant value for cryo-EM/cryo-ET studies of HIV and HIV VLPs because of the fact that the virus and VLPs have a "spherical" shape and a diameter of ~125 nm, which tends to encourage them to aggregate and cluster near the edges of the Quantifoil grid holes (Fig. 2B). Cryo-ET data were collected of HIV VLPs on both regular cryo-grids and cryo-AG to determine whether the presence of the monolayer would impact individual image quality and subsequent achievable resolution of the 3D reconstructions. In the 3D reconstructions, we were able to resolve the Gag polyprotein shells that are a structural hallmark of immature HIV VLPs or immature HIV virions (data not shown). This information showed that neither the AG lipid layer nor the molecular adaptors reduced the quality of the structural information obtainable from the HIV VLPs.

Orthomyxoviruses

The *Orthomyxoviridae* family of viruses includes the human pathogens influenza A, B, and C. Viruses from this family exhibit a broad range of morphologies that encompass the small and mostly spherical to the long and filamentous varieties. *Orthomyxoviridae* viruses are ideal candidates to test the applicability of AG for capturing viruses with greater morphological heterogeneity than the HIV VLPs and lesser pleomorphic character than MeV. Influenza A/PR8 7:1 (H1N1) virus was used in the AG experiment because preparations of this strain contain a mixture of both spherical and filamentous virus particles (Fig. 3). Similar to the HIV CD84 VLPs, influenza A/PR8 7:1 particles exhibited a dependency on attachment to the AG when the percentage of the Ni-NTA was varied in the monolayer from 2 to 50% (Figs. 3B–3E; Supplementary Table 4). Only intact particles exhibiting the characteristic influenza morphology and visible, well-ordered glycoproteins were categorized as a "virus." Particles that were broken and/or without glycoproteins were classified as "other particles."

We assessed if elimination of the Protein A-His or the antibody resulted in a clear decrease or absence of captured influenza A/PR8 7:1 particles, the removal of either component abolished viral particle adherence (Supplementary Figs. 3A, 3B; Supplementary Table 4). At the same time, we also determined that influenza A/PR8 7:1 particles were readily eluted from the AG with the addition of 600 mM imidazole (Supplementary Fig. 3C). After imidazole treatment, the monolayer remained functional because influenza A/PR8 7:1 particles were able to reattach to the AG monolayer surface (Supplementary Fig. 3D; Supplementary Table 4). The level of influenza A/PR8 7:1 particle attachment was reduced after imidazole treatment (26.8 ± 8.11) when compared to the 20% AG values (63.0 ± 8.72). This reduction could be because of chemical or physical disruption of the lipid monolayer and the Ni-NTA active groups. Using AG to capture influenza A/PR8 7:1 particles onto cryo-EM grids (Figs. 4D, 4E; Supplementary Table 5) did not produce as significant an increase in the numbers of captured viral particle as it did for HIV VLPs (Supplementary Table 3). However, there was a greater dispersion and even distribution of the viral particles on the cryo-AG when compared to standard cryo-EM grids (Figs. 4A, 4B), which is also advantageous for cryo-EM studies (Figs. 4D, 4E).

Paramyxoviruses

Paramyxoviruses are significant human pathogens known for their extreme pleomorphicity and difficult purification.

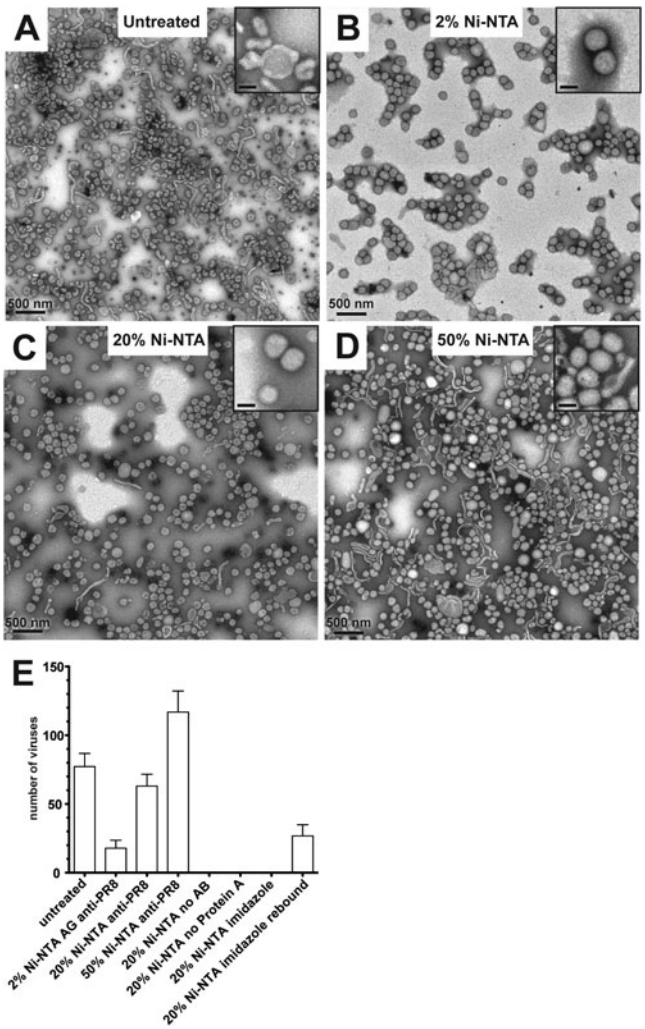

Figure 3. Transmission electron microscopy images of negatively stained influenza A/PR8 7:1. **A:** Influenza A/PR8 7:1 particles from the resuspended pellet. **B:** Influenza A/PR8 7:1 particles captured on a 2% nickel-nitrilotriacetic acid (Ni-NTA) affinity grid (AG) using an anti-PR8 polyclonal antibody (1:500). **C:** Influenza A/PR8 7:1 particles captured on a 20% Ni-NTA AG using an anti-PR8 polyclonal antibody (1:500). **D:** Influenza A/PR8 particles captured on a 50% Ni-NTA AG using an anti-PR8 polyclonal antibody (1:500). **E:** Accounting of the number of influenza A/PR8 7:1 particles adsorbed to untreated and AG EM grids. The AGs recruited influenza A/PR8 7:1 particles in a manner that was proportional to the percentage of Ni-NTA present in the lipid monolayer. AG prepared without the anti-PR8 polyclonal antibody or the Protein A-His did not recruit particles to the grid surface. Treatment of the AG with 600 mM imidazole resulted in the elution of particles previously bound to the AG surface. Influenza A/PR8 7:1 particles were able to bind to the imidazole-treated surface. Images were acquired at 4,000 and 12,000× (insets) magnifications. Scale bars are 500 and 100 nm (insets).

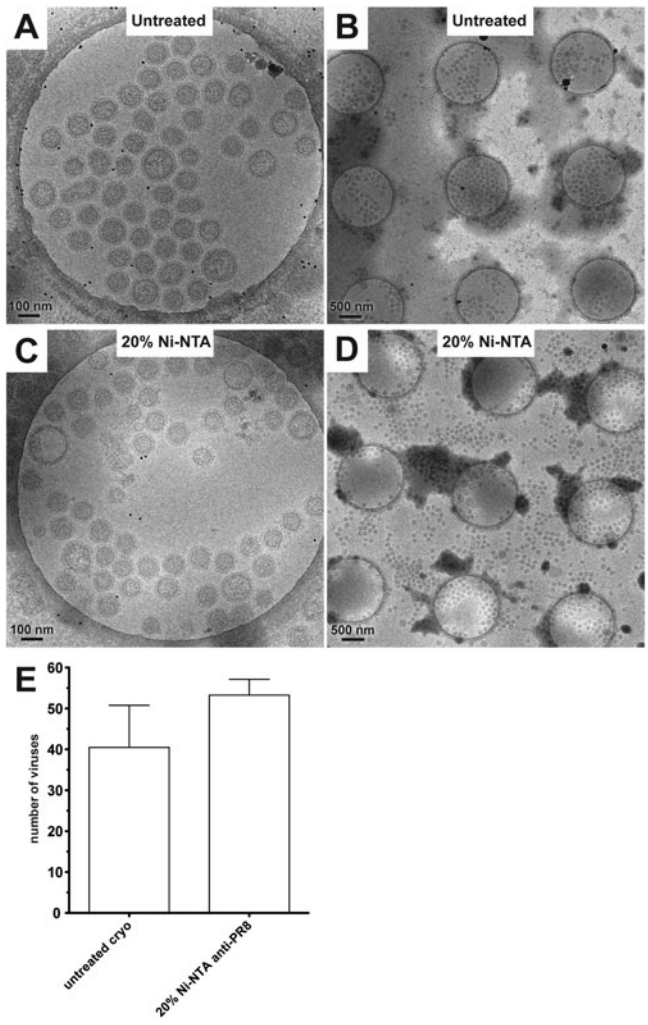

Figure 4. Cryo-electron microscopy (cryo-EM) images of influenza A/PR8 7:1. **A, B:** Cryo-EM images of influenza A/PR8 7:1 particles applied to a standard cryo-EM grid. **C, D:** Cryo-EM images of influenza A/PR8 7:1 particles captured on a 20% nickel-nitrilotriacetic acid (Ni-NTA) cryo-affinity grid (cryo-AG) with an anti-PR8 polyclonal antibody (1:100). **E:** Measurement of influenza A/PR8 7:1 particles present on untreated and AG cryo-EM grids. Untreated EM grids adsorbed fewer influenza A/PR8 7:1 particles than the 20% Ni-NTA AG cryo-EM grid. Images were acquired at 30,000× (**A, C**) and 4,000× (**B, D**) magnifications. Scale bar: (**A, C**) 100 nm and (**B, D**) 500 nm.

Viruses from the *Paramyxoviridae* family display a broad range of shapes and sizes, which have lead to significant controversies regarding whether all the morphologies reported represent true viruses or if some may be defective interfering particles (Hall et al., 1974; Maeda et al., 1978; Valdovinos & Gomez, 2003). A major hindrance to resolving this debate is the inability to obtain highly concentrated and pure viral samples for conventional TEM or cryo-EM structural studies. Therefore, the optimization of AG virus purification will be a practical solution for improving the success of EM-based studies of paramyxoviruses.

MeV

MeV displays the greatest degree of structural pleomorphicity of all the viruses examined by our group. In addition, the majority of MeV progeny particles remain cell associated, which increases the possibility of the incorporation of vesicles and other cellular debris decorated with the viral glycoproteins into the "purified" virus preparation. Both of these

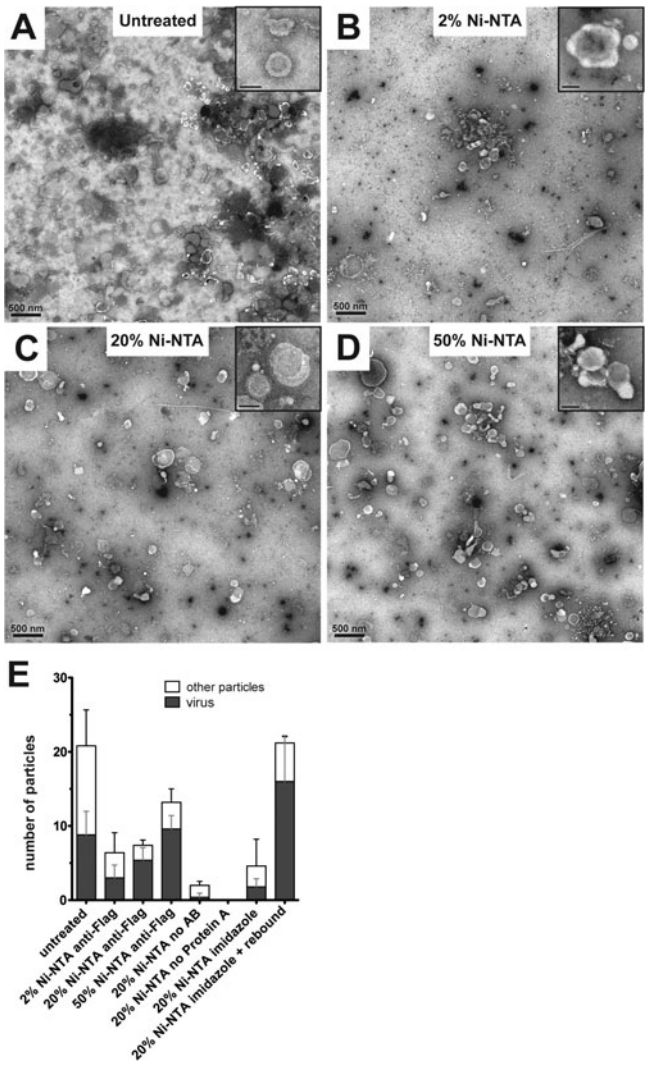

Figure 5. Transmission electron microscopy images of negatively stained recMeV-H-Edm$_{3\times Flag}$ particles. **A:** recMeV-H-Edm$_{3xFlag}$ particles from the resuspended pellet. **B:** recMeV-H-Edm$_{3xFlag}$ particles captured on a 20% nickel-nitrilotriacetic acid (Ni-NTA) affinity grid (AG) using an anti-Flag antibody (1:500). **C:** Quantification of recMeV-H-Edm$_{3xFlag}$ particles (gray) and other particles (white) present on untreated and AG electron microscopy (EM grids). Untreated EM grids adsorbed more total particles than the three AGs. The AGs recruited recMeV-H-Edm$_{3xFlag}$ particles in a stepwise fashion that was proportional to the percentage of Ni-NTA present in the lipid monolayer. The quantity of other particles present on all the AGs was greatly reduced. AG prepared without the antibody did not recruit particles to the grid surface. Treatment of the AG with 600 mM imidazole resulted in the elution of particles previously bound to the AG surface. Particles could be rebound to the AG after imidazole treatment. (**A, B**) were acquired at 4,000 and 12,000× (insets) magnifications. Scale bars are 500 and 100 nm (insets).

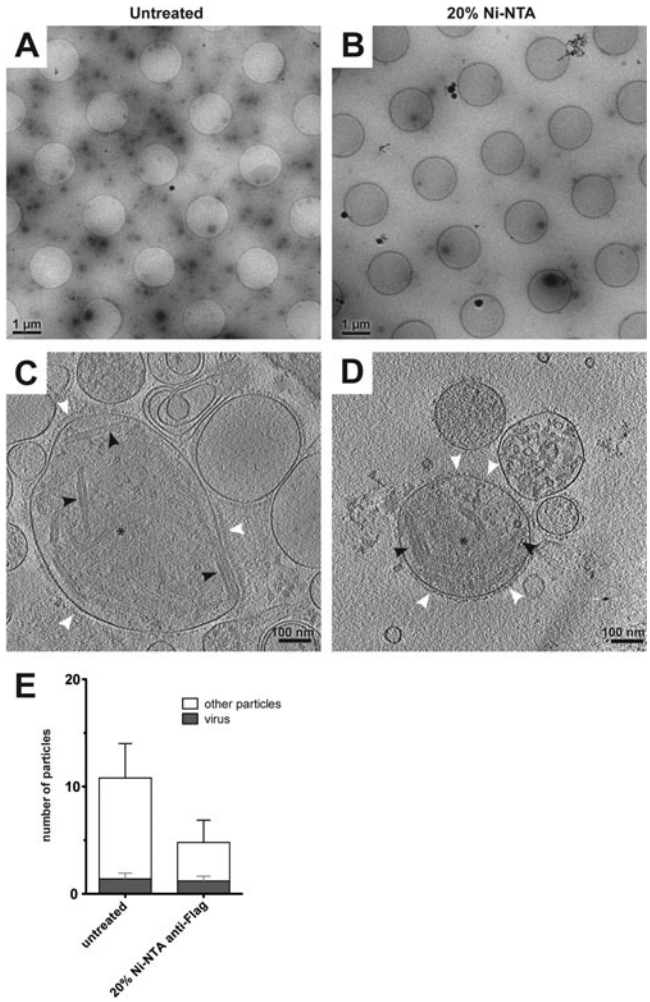

Figure 6. Cryo-electron microscopy (cryo-EM) images and cryo-electron tomography (cryo-ET) reconstructions of recMeV-H-Edm$_{3xFlag}$ particles. **A:** Cryo-EM images of recMeV-H-Edm$_{3xFlag}$ particles applied to a standard cryo-EM grid. **B:** recMeV-H-Edm$_{3xFlag}$ particles captured on a 20% nickel-nitrilotriacetic acid (Ni-NTA) cryo-affinity grid (AG) with an anti-Flag antibody (1:500). **C:** 7.6 nm slices through reconstructions of recMeV-H-Edm$_{3xFlag}$ particles on standard cryo-EM grids. **D:** 7.6 nm slices through reconstructions of recMeV-H-Edm$_{3xFlag}$ particles on a 20% Ni-NTA cryo-AG with an anti-Flag antibody (1:500). **C, D:** Black asterisks denote recMeV-H-Edm$_{3xFlag}$ particles, white arrowheads point to the surface glycoproteins, and black arrowheads mark the RNP. **E:** Measurement of recMeV-H-Edm$_{3xFlag}$ particles (gray) and other particles (white) present on untreated and AG cryo-EM grids. Untreated EM grids adsorbed more particles of all types. The 20% Ni-NTA AG recruited recMeV-H-Edm$_{3xFlag}$ particles to the cryo-EM grid and reduced the quantity of other particles present. Scale bar: (**A, B**) 1 μm and (**C, D**) 100 nm.

attributes make cryo-EM structural analyses of MeV extremely challenging. In our study, we used the AG techniques for MeV in order to increase the number of virus particles adsorbed to the grid surface while simultaneously reducing the quantity of other contaminants on the grid so that the virus sample would be more feasible for ultrastructural analysis. RecMeV-H-Edm$_{3\times FLAG}$ (MeV-Flag) was engineered to display the Flag epitope-tag at a membrane-distal position of the H protein head domain. The inclusion of the Flag-tag does not impact virus infectivity (Plemper et al., 2001) or morphology (Figs. 5, 6C, 6D). The addition of the Flag-tag made the virus more suitable for affinity purification.

Using a high-affinity anti-Flag antibody, particles were successfully recruited to the AG (Figs. 5B–5D). Due to the unavoidable presence of glycoprotein-studded vesicles in the preparation, a mixture of MeV particles and vesicles did adhere to the AG. However, there was a significant decrease in the cellular debris localized to the AG surfaces when compared with the conventional EM grids (Fig. 5A). This indicated that only particles, which had viral glycoproteins on their surface, were able to bind to and remain associated with the AG.

We quantified the number of MeV-Flag particles and other particles present on untreated EM grids and on the AG to further confirm the utility of the AG technique when used to capture MeV-Flag particles on EM grids (Fig. 5E; Supplementary Table 6). Only particles which displayed the characteristic MeV-Flag morphology of an intact viral envelope that were highly decorated with the virus-specific surface glycoproteins were counted as "virus particles." Particles lacking any of the features mentioned were categorized as "other particles." For better scoring, we used higher magnification images of the assessed particles as further confirmation. Our analysis revealed that there were, on average, greater numbers of nonviral particles (12.0 ± 4.85) present than the MeV-Flag particles (8.8 ± 3.19) on the untreated EM grids. However, on the AG, while there were fewer particles in total, the quantity of identifiable MeV-Flag particles was greater compared to the amount of other particles on the grids. We determined that when the amount of the Ni-NTA lipid was increased in the affinity monolayer the recruitment of the MeV-Flag particles was enhanced, as was measured for 2% (3.0 ± 1.73), 20% (5.4 ± 2.0), and 50% (9.6 ± 3.6) Ni-NTA lipid. Interestingly, the amount of the other particles present on the AG surface was low, with the mean number of particles remaining at ∼3 (Fig. 5E; Supplementary Table 6). We did observe that the proportionality between the percentage of the Ni-NTA lipid in the monolayer and MeV-Flag particle recruitment was not as pronounced as it was for the HIV VLPs (Fig. 1; Supplementary Fig. 1; Supplementary Tables 1, 2) or the influenza particles (Fig. 3; Supplementary Table 4), this could be attributed to several aspects. First, the significant structural heterogeneity of the MeV-Flag particles could have impacted the orientation and exposure of the H-Flag epitope-tag to the AG surface, thereby limiting the viral particles' degree of association with the grid surface. Second, the lower titer of the MeV-Flag particles ($\sim 10^7$ $TCID_{50}$ units/mL) combined with the higher quantity of background material when compared to that of either the highly pure and concentrated influenza particles ($\sim 10^{8-10}$ PFU/mL) or HIV VLPs (100 μg/mL of p24 and 5 μg/mL of gp120) could have limited the adherence of MeV-Flag particles to the AG. We determined that removing the incorporation of the antibody or the Protein A from the AG experiment resulted in the loss of MeV-Flag particle attachment to the AG. We were able to elute MeV-Flag particles from the AG with the addition of 600 mM imidazole. Both attributes suggest that the interaction between MeV-Flag particles and the monolayer was maintained by the antibody-Protein A-His-Ni-NTA complex (Fig. 5E; Supplementary Fig. 4; Supplementary Table 6). Subsequent to treatment of the AG with imidazole, we examined if the AG surface would continue to support the recruitment of MeV-Flag particles. After the imidazole elution MeV-Flag particles were able to attach to the 20% Ni-NTA monolayer when Protein A and the anti-Flag antibody was applied (16 ± 6.2) and the number of nonviral particles remained low (5.2 ± 0.8) (Supplementary Table 6). This suggested that the lipid monolayer remained intact and the preferential binding activity supported by the 20% Ni-NTA AG was stable.

Applying the AG technique to cryo-grids resulted in the presence of fewer particles of all types on the grids (Figs. 6B, 6D; Supplementary Table 7), and of those particles present, there were greater numbers of particles with surface glycoproteins and a visible RNP complex in the virus interior. This suggests that large fractions of cellular debris and vesicles were removed from the cryo-AG. Cryo-ET data were collected on MeV particles on both regular cryo-grids (Fig. 6C) and cryo-AG (Fig. 6D) to determine whether the presence of the monolayer would impact individual image quality and subsequent achievable resolution of the 3D reconstructions. From both grid types, after the generation of the reconstructions, we identified individual glycoproteins on the surface of the virions (Fig. 6, white arrowheads), the viral membrane, and the RNP structure inside of the particles (Fig. 6, black arrowheads). This indicated that the addition of the lipid layer or the molecular adaptors did not decrease signal from the viral macromolecules or introduce noise to the images. The RNP structure was double layered, which suggested that the internal layer represents the RNP and the viral matrix protein may form a shell encasing the RNP. This finding supports the previous reports of MeV generating a combined RNP–matrix complex (Liljeroos et al., 2011).

Conclusions

Structural studies are fundamental for the development of antivirals that target many families of enveloped viruses. Valuable information is found at both high and intermediate resolutions, specifically how individual macromolecular interactions contribute to dramatic alterations of overall viral organization or subtle changes such as exposure of specific epitopes. Enveloped viruses exhibit great structural heterogeneity; therefore the best methods for the analysis of intact viral particles are cryo-EM and cryo-ET. In this work, a recent technology known as the "AG" was optimized for the capture of enveloped viruses directly onto EM grids. Before the initiation of these studies, three additional experimental factors were considered. First, the availability of a high-affinity antibody, which targets a well-exposed epitope on each of the viruses, was required for the success of the technique. Second, the quantity of the antibody used needed optimization. Finally, it was necessary to either avoid or limit the use of sucrose, detergents, or

harsh chemicals during specimen preparation because minute quantities of these compounds would destroy the lipid monolayer.

Viruses from three enveloped virus families, *Retroviridae*, *Orthomyxoviridae*, and *Paramyxoviridae* were chosen because: (1) the families contain a number of highly infectious pathogens to humans and animals and (2) they represent the significant range of structural heterogeneity present amongst viruses. The individual viruses studied were: HIV CD84 VLPs, influenza A, and MeV. We demonstrated that the AG could selectively capture all of the viruses; the antibody-Protein A-His-Ni-NTA complex maintained the interaction with the particles; and this interaction was strong enough to maintain the coordination of the viruses to the cryo-AG. We have observed a broad range of virus morphologies in the three virus samples and noted that an increase in virus pleomorphism coincides with an overall lowered capturing efficiency to the AG. Interestingly, the large, pleomorphic virus particles can be recruited to higher Ni-NTA-containing monolayers. An example is the filamentous form of influenza A/PR8 7:1 that is underrepresented on the 2% Ni-NTA AG (Fig. 3B), while on the 50% Ni-NTA AG their presence is comparable to the untreated grids (Figs. 3D and 3A, respectively). The negative impact of virus pleomorphism on the total number of captured virus particles is more pronounced under cryo-conditions, as noted for influenza A/PR8 7:1 (Fig. 4) and MeV-Flag (Fig. 6). One possible explanation for the observed reduction in large, pleomorphic virus numbers under cryo-conditions could be that the interactions that support the adherence of the viruses to the 20% Ni-NTA AG monolayer are too weak to be maintained against the force of blotting during grid vitrification. Conversely, the viruses adsorbed to the negative stain 20% Ni-NTA AG monolayer are able to withstand the washing steps that are commonly used. Large virus particle attachment could be improved by using 50% Ni-NTA AG monolayer on the cryo-AG. The increased Ni-NTA in the monolayer may also promote the recruitment of a greater number of pleomorphic viruses. That said, for all the enveloped viruses examined, an improvement was observed in both viral particle distribution and viral particle numbers on both the negatively stained and cryo-EM AGs. The gain was most noticeable in the negative stain AG experiments. However, for cryo-EM, the slightest enhancement to virus distribution and virus particles quantity combined with the reduction of cell-derived contaminants on the cryo-grid can significantly impact the likelihood of a successful study (HIV—Fig. 2, influenza A/PR8 7:1—Fig. 4, MeV-Flag—Fig. 6). The balance between the quantity of virus particles and cellular debris present on all the grid types studied was best illustrated with MeV-Flag (Figs. 5, 6; Supplementary Tables 6, 7). We also found that cryo-ET tilt series collected of viruses on cryo-AGs are suitable for further high-resolution structural studies and that the additional lipid layer does not diminish the valuable signal from the sample or produce noticeable background noise.

In this study, we were not explicitly concerned with possible conformational changes of the surface glycoprotein structures upon their binding with the antibody. If the aim is to determine the native structure of the surface glycoproteins, a promising substitute to conventional antibody-to-glycoprotein interactions may be to employ alternative anchors for the affinity immobilization. For example, in our study of the HIV CD84 VLPs, two binding sites were available, HIV Env and a cellular glycoprotein, CD84. In both cases, we observed selective capture of the HIV VLPs to the AG, but we could be assured that when using the CD84 antibody capture, the structure of HIV Env would not be altered (Supplementary Fig. 1). The other approach is to engineer viruses with extended His-tags anchored to the surface glycoproteins. To this end, we examined two His-tagged MeV mutants in which the His-tags were placed on one of the surface glycoproteins. Unfortunately, our results were not consistent, suggesting that there may be other factors that limit its applicability at this time including possible steric-hindrances from interactions between the two surface glycoproteins or flexibility from the extended architecture of the His-tagged glycoprotein (data not shown). We continue to develop the AG method to improve the success of virus capture without disrupting the lipid monolayer or the structure of the viral glycoproteins.

As with many methods that are in development, there are technical challenges associated with the AG process. However, we have illustrated the significant improvements that can be realized by using AG for conventional TEM and cryo-EM analyses of enveloped viruses. The benefits of the AG in TEM imaging are especially true for viruses in which the production of a suitable EM sample is difficult because of limited quantities of the virus; the inability to produce high-purity virus stocks; or information regarding virus sample quality or quantity is unavailable. Due to the significant impact that employing AG techniques will afford to the purification of enveloped viruses directly to EM grids, we propose that this method is a powerful future tool for ultrastructural analyses of viruses.

Acknowledgments

The authors thank Dr. Leon De Masi for providing reagents and support during the preparation of the manuscript. We would like to thank Dr. Jason Hammonds for the anti-Env polyclonal antibody and Dr. Philip Santangelo for the anti-NDV polyclonal antibody. We also thank Ms. Jeannette Taylor and Ms. Hong Yi of the Emory University Robert P. Apkarian Integrated Electron Microscopy Core for assistance. This work was supported in part by Emory University, Children's Healthcare of Atlanta, the Center for AIDS Research at Emory University (P30 AI050409), and the Georgia Research Alliance to E.R.W.; NSF grant 0923395 to E.R.W; and public health service grants AI101775 to E.R.W, AI058828 to P.W.S., and AI083402 to R.K.P. from the NIH/NIAID; USDA_ARS CRIS project number 66612-32000-064 to C.L.A.; and Centers for Excellence in Influ-

enza Research and Surveillance (CEIRS) contract number HHSN266200700006C to J.S. and D.A.S.

References

Briggs, J.A., Grunewald, K., Glass, B., Forster, F., Krausslich, H.G. & Fuller, S.D. (2006*a*). The mechanism of HIV-1 core assembly: Insights from three-dimensional reconstructions of authentic virions. *Structure* **14**, 15–20.

Briggs, J.A., Johnson, M.C., Simon, M.N., Fuller, S.D. & Vogt, V.M. (2006*b*). Cryo-electron microscopy reveals conserved and divergent features of Gag packing in immature particles of Rous sarcoma virus and human immunodeficiency virus. *J Mol Biol* **355**, 157–168.

Butan, C., Winkler, D.C., Heymann, J.B., Craven, R.C. & Steven, A.C. (2008). RSV capsid polymorphism correlates with polymerization efficiency and envelope glycoprotein content: Implications that nucleation controls morphogenesis. *J Mol Biol* **376**, 1168–1181.

Calder, L.J., Wasilewski, S., Berriman, J.A. & Rosenthal, P.B. (2010). Structural organization of a filamentous influenza A virus. *Proc Natl Acad Sci USA* **107**, 10685–10690.

Carlson, L.A., Briggs, J.A., Glass, B., Riches, J.D., Simon, M.N., Johnson, M.C., Muller, B., Grunewald, K. & Krausslich, H.G. (2008). Three-dimensional analysis of budding sites and released virus suggests a revised model for HIV-1 morphogenesis. *Cell Host Microbe* **4**, 592–599.

de Marco, A., Davey, N.E., Ulbrich, P., Phillips, J.M., Lux, V., Riches, J.D., Fuzik, T., Ruml, T., Krausslich, H.G., Vogt, V.M. & Briggs, J.A. (2010). Conserved and variable features of Gag structure and arrangement in immature retrovirus particles. *J Virol* **84**, 11729–11736.

Fodor, E., Devenish, L., Engelhardt, O.G., Palese, P., Brownlee, G.G. & Garcia-Sastre, A. (1999). Rescue of influenza A virus from recombinant DNA. *J Virol* **73**, 9679–9682.

Fontana, J., Cardone, G., Heymann, J.B., Winkler, D.C. & Steven, A.C. (2012). Structural changes in influenza virus at low pH characterized by cryo-electron tomography. *J Virol* **86**, 2919–2929.

Gias, E., Nielsen, S.U., Morgan, L.A. & Toms, G.L. (2008). Purification of human respiratory syncytial virus by ultracentrifugation in iodixanol density gradient. *J Virol Methods* **147**, 328–332.

Gilmore, B.L., Showalter, S.P., Dukes, M.J., Tanner, J.R., Demmert, A.C., McDonald, S.M. & Kelly, D.F. (2013). Visualizing viral assemblies in a nanoscale biosphere. *Lab Chip* **13**, 216–219.

Hall, W.W., Martin, S.J. & Gould, E. (1974). Defective interfering particles produced during the replication of measles virus. *Med Microbiol Immunol* **160**, 155–164.

Hammonds, J., Chen, X., Zhang, X., Lee, F. & Spearman, P. (2007). Advances in methods for the production, purification, and characterization of HIV-1 Gag-Env pseudovirion vaccines. *Vaccine* **25**, 8036–8048.

Harris, A., Cardone, G., Winkler, D.C., Heymann, J.B., Brecher, M., White, J.M. & Steven, A.C. (2006). Influenza virus pleiomorphy characterized by cryoelectron tomography. *Proc Natl Acad Sci USA* **103**, 19123–19127.

Heymann, J.B., Butan, C., Winkler, D.C., Craven, R.C. & Steven, A.C. (2008). Irregular and semi-regular polyhedral models for Rous sarcoma virus cores. *Comput Math Methods Med* **9**, 197–210.

Hicar, M.D., Chen, X., Briney, B., Hammonds, J., Wang, J.J., Kalams, S., Spearman, P.W. & Crowe, J.E., Jr. (2010). Pseudovirion particles bearing native HIV envelope trimers facilitate a novel method for generating human neutralizing monoclonal antibodies against HIV. *J Acquir Immune Defic Syndr* **54**, 223–235.

Keller, P.W., Adamson, C.S., Heymann, J.B., Freed, E.O. & Steven, A.C. (2011). HIV-1 maturation inhibitor bevirimat stabilizes the immature Gag lattice. *J Virol* **85**, 1420–1428.

Kelly, D.F., Abeyrathne, P.D., Dukovski, D. & Walz, T. (2008*a*). The affinity grid: A pre-fabricated EM grid for monolayer purification. *J Mol Biol* **382**, 423–433.

Kelly, D.F., Dukovski, D. & Walz, T. (2008*b*). Monolayer purification: A rapid method for isolating protein complexes for single-particle electron microscopy. *Proc Natl Acad Sci USA* **105**, 4703–4708.

Kelly, D.F., Dukovski, D. & Walz, T. (2010*a*). A practical guide to the use of monolayer purification and affinity grids. *Methods Enzymol* **481**, 83–107.

Kelly, D.F., Dukovski, D. & Walz, T. (2010*b*). Strategy for the use of affinity grids to prepare non-His-tagged macromolecular complexes for single-particle electron microscopy. *J Mol Biol* **400**, 675–681.

Kremer, J.R., Mastronarde, D.N. & McIntosh, J.R. (1996). Computer visualization of three-dimensional image data using IMOD. *J Struct Biol* **116**, 71–76.

Lee, K.K. (2010). Architecture of a nascent viral fusion pore. *EMBO J* **29**, 1299–1311.

Liljeroos, L., Huiskonen, J.T., Ora, A., Susi, P. & Butcher, S.J. (2011). Electron cryotomography of measles virus reveals how matrix protein coats the ribonucleocapsid within intact virions. *Proc Natl Acad Sci USA* **108**, 18085–18090.

Liljeroos, L., Krzyzaniak, M.A., Helenius, A. & Butcher, S.J. (2013). Architecture of respiratory syncytial virus revealed by electron cryotomography. *Proc Natl Acad Sci USA* **110**, 11133–11138.

Loney, C., Mottet-Osman, G., Roux, L. & Bhella, D. (2009). Paramyxovirus ultrastructure and genome packaging: Cryo-electron tomography of sendai virus. *J Virol* **83**, 8191–8197.

Maeda, A., Suzuki, Y. & Matsumoto, M. (1978). Isolation and characterization of defective interfering particle of Newcastle disease virus. *Microbiol Immunol* **22**, 775–784.

Mastronarde, D.N. (2005). Automated electron microscope tomography using robust prediction of specimen movements. *J Struct Biol* **152**, 36–51.

Mbiguino, A. & Menezes, J. (1991). Purification of human respiratory syncytial virus: Superiority of sucrose gradient over percoll, renografin, and metrizamide gradients. *J Virol Methods* **31**, 161–170.

McGinnes, L.W., Pantua, H., Reitter, J. & Morrison, T.G. (2006). Newcastle disease virus: Propagation, quantification, and storage. *Curr Protoc Microbiol* Chapter 15, Unit 15F, 12.

Ono, N., Tatsuo, H., Hidaka, Y., Aoki, T., Minagawa, H. & Yanagi, Y. (2001). Measles viruses on throat swabs from measles patients use signaling lymphocytic activation molecule (CDw150) but not CD46 as a cellular receptor. *J Virol* **75**, 4399–4401.

Plemper, R.K., Hammond, A.L. & Cattaneo, R. (2001). Measles virus envelope glycoproteins hetero-oligomerize in the endoplasmic reticulum. *J Biol Chem* **276**, 44239–44246.

Sugita, Y., Noda, T., Sagara, H. & Kawaoka, Y. (2011). Ultracentrifugation deforms unfixed influenza A virions. *J Gen Virol* **92**, 2485–2493.

Tanner, J.R., Degen, K., Gilmore, B.L. & Kelly, D.F. (2012). Capturing RNA-dependent pathways for cryo-EM analysis. *Comput Struct Biotech J* **1**, e201204003-1–6.

Valdovinos, M.R. & Gomez, B. (2003). Establishment of respiratory syncytial virus persistence in cell lines: Association with defective interfering particles. *Intervirology* **46**, 190–198.

Wickramasinghe, S.R., Kalbfuss, B., Zimmermann, A., Thom, V. & Reichl, U. (2005). Tangential flow microfiltration and ultrafiltration for human influenza A virus concentration and purification. *Biotechnol Bioeng* **92**, 199–208.

Wright, E.R., Schooler, J.B., Ding, H.J., Kieffer, C., Fillmore, C., Sundquist, W.I. & Jensen, G.J. (2007). Electron cryotomography of immature HIV-1 virions reveals the structure of the CA and SP1 Gag shells. *EMBO J* **26**, 2218–2226.

Yamaguchi, M., Danev, R., Nishiyama, K., Sugawara, K. & Nagayama, K. (2008). Zernike phase contrast electron microscopy of ice-embedded influenza A virus. *J Struct Biol* **162**, 271–276.

Zhang, L., Hernan, R. & Brizzard, B. (2001). Multiple tandem epitope tagging for enhanced detection of protein expressed in mammalian cells. *Mol Biotechnol* **19**, 313–321.